Geochemistry, Geophysics, Geosystems®

AGU ADVANCING EARTH AND SPACE SCIENCE

RESEARCH ARTICLE
10.1029/2022GC010543

Key Points:

- Reactive Fe is transferred from river-derived Fe oxides into Fe-containing silicate minerals during early diagenesis
- Standard sequential extraction schemes do not separate Fe oxides and carbonates from authigenic silicate minerals in Amazon shelf sediments
- Terrigenous supply of reactive Fe and reverse weathering need to be considered in the interpretation of sedimentary Fe speciation

Supporting Information:

Supporting Information may be found in the online version of this article.

Correspondence to:

P. Vosteen and F. Scholz,
pvosteen@geomar.de;
fscholz@geomar.de

Citation:

Vosteen, P., Spiegel, T., Gledhill, M., Frank, M., Zabel, M., & Scholz, F. (2022). The fate of sedimentary reactive iron at the land-ocean interface: A case study from the Amazon shelf. *Geochemistry, Geophysics, Geosystems*, *23*, e2022GC010543. https://doi.org/10.1029/2022GC010543

Received 25 MAY 2022
Accepted 26 OCT 2022

The Fate of Sedimentary Reactive Iron at the Land-Ocean Interface: A Case Study From the Amazon Shelf

Paul Vosteen[1], Timo Spiegel[1], Martha Gledhill[1], Martin Frank[1], Matthias Zabel[2], and Florian Scholz[1]

[1]GEOMAR Helmholtz Centre for Ocean Research Kiel, Kiel, Germany, [2]MARUM Center for Marine Environmental Sciences, Bremen, Germany

Abstract Reactive iron (Fe) oxides in marine sediments may represent a source of bioavailable Fe to the ocean via reductive dissolution and sedimentary Fe release or can promote organic carbon preservation and long-term burial. Furthermore, enrichments of reactive Fe (sum of Fe oxides, carbonates and sulfides normalized to total Fe) in ancient sediments are utilized as a paleo-proxy for anoxic conditions. Considering the general importance of reactive Fe oxides in marine biogeochemistry, it is important to quantify their terrestrial sources and fate at the land-ocean interface. We applied sequential Fe extractions to sediments from the Amazon shelf to investigate the transformation of river-derived Fe oxides during early diagenesis. We found that ~22% of the Amazon River-derived Fe oxides are converted to Fe-containing clay minerals in Amazon shelf sediments. The incorporation of reactive Fe into authigenic clay minerals (commonly referred to as reverse weathering) is substantiated by the relationship between Fe oxide loss and potassium (K) uptake from sedimentary pore waters, which is in agreement with the previously reported Fe/K stoichiometry of authigenic clay minerals. Mass balance calculations suggest that widely applied sequential extractions do not separate Fe-rich authigenic clay minerals from reactive Fe oxides and carbonates. We conclude that the balance between terrestrial supply of reactive Fe and reverse weathering in continental margin sediments has to be taken into account in the interpretation of sedimentary Fe speciation data.

1. Introduction

Biogeochemically reactive iron (Fe) species in marine sediments play an important role in the global carbon cycle. Primary productivity in as much as half of the world's ocean is controlled by the availability of Fe (Boyd & Ellwood, 2010; Tagliabue et al., 2017). Reductive dissolution of Fe oxide minerals in anoxic marine sediments coupled to transport of dissolved Fe (Fe^{2+}) across the sediment-water interface represents an important source of bioavailable Fe to the ocean (Dale et al., 2015; Elrod et al., 2004; Scholz, 2018; Tagliabue et al., 2016). Furthermore, Fe oxide minerals in marine sediments interact with organic material; The association of organic material with Fe oxide minerals reduces its reactivity and thus promotes preservation and long-term removal of carbon from Earth surface reservoirs via burial in marine sediments (Faust et al., 2021; Hemingway et al., 2019; Lalonde et al., 2012).

The concentration of reactive Fe in marine sediments is also employed as a paleo-redox proxy (Poulton & Canfield, 2011). In oxygen-deficient ocean regions, large-scale transport of sediment-derived (or hydrothermally sourced) Fe in the water column can generate sedimentary enrichments of reactive Fe at those locations where dissolved Fe is re-precipitated (Lyons & Severmann, 2006; Raiswell & Anderson, 2005; Raiswell et al., 2018; Scholz, Severmann, McManus, & Hensen, 2014). This mechanism (so-called Fe shuttle) results in a focused deposition of reactive Fe and thus generates an elevated proportion of reactive Fe within the total Fe pool in the Fe sink areas compared to the terrigenous background sedimentation. When detected in the geological record, this reactive Fe speciation signature is generally interpreted as an indication for anoxic conditions in the water column at the time of deposition (Poulton & Canfield, 2011; Poulton et al., 2010; Raiswell et al., 2018). However, this approach requires that the contemporary terrigenous flux of reactive Fe is known or has remained constant over the course of Earth's history. Considering the general importance of reactive Fe in marine biogeochemistry and paleo-environmental research, a sound understanding of external sources of reactive Fe to the ocean and how reactive Fe is modified at the land-ocean interface is required.

Reactive Fe has traditionally been defined as the fraction of Fe in marine sediment (chiefly Fe oxides), which readily reacts with hydrogen sulfide originating from bacterial sulfate reduction to form Fe sulfide minerals and

eventually pyrite (Berner, 1970, 1984; Canfield, 1989; Poulton & Canfield, 2011). Nowadays, the highly reactive Fe fraction of a sediment sample (Fe_{HR}) is commonly quantified by applying a standardized sequential extraction scheme (Alcott et al., 2020; Poulton & Canfield, 2005). Following this approach, the term Fe_{HR} represents the operationally defined sum of Fe associated with carbonate minerals (e.g., siderite, ankerite), reducible Fe oxides (ferrihydrite, goethite, and hematite), magnetite and pyrite (Poulton & Canfield, 2005).

The most important external source of particulate reactive Fe to the ocean is chemical weathering on the continents and riverine transport of weathering products (Poulton & Raiswell, 2002; Raiswell, 2006). During chemical weathering, ferrous Fe(II) in unreactive silicate minerals (e.g., olivine, biotite, and pyroxene) is oxidized and reactive ferric Fe(III) oxide minerals are precipitated (Blume, 1988; Schwertmann, 1988). These Fe oxides are then eroded along with other particles and transported as riverine particulate matter (Poulton & Raiswell, 2002). The highest proportions of reactive Fe oxides within the total Fe pool are found in riverine particles originating from regions with high runoff and intense chemical weathering in the riverine catchment area (Canfield, 1997; Poulton & Raiswell, 2002). In a seminal study, Poulton and Raiswell (2002) demonstrated that river suspended particles are generally characterized by higher proportions of reactive Fe oxides within the total Fe pool than continental margin sediments. They reported a globally averaged reactive Fe to total Fe ratio in river particulates of 0.43 ± 0.03, whereas average continental margin sediments with oxic bottom waters (24 locations off Europe and North America; Raiswell & Canfield, 1998) were characterized by a lower ratio of 0.28 ± 0.06 (Poulton & Raiswell, 2002). Conversion of Fe oxide to Fe sulfide minerals during early diagenesis was generally not sufficient to explain the offset in reactive Fe between riverine particles and marine sediments. Therefore, Poulton and Raiswell (2002) argued that particulate reactive Fe must be demobilized at the land-ocean interface and stored in inner shore sediments (i.e., within estuaries, tidal flats, and salt marshes). This process could take place together with dissolved Fe removal along the estuarine salinity gradient, which is mediated by aggregation of Fe colloids with organic matter and cations contained in seawater (Mayer, 1982; Moore et al., 1979; Sholkovitz, 1978).

Another potential but yet unexplored explanation for a lower proportion of reactive Fe in marine sediments compared to river suspended particles is a process called reverse weathering. During this process, terrigenous Fe oxide minerals react with biogenic silica and cations dissolved in seawater to form authigenic clay minerals such as glauconite or potassium-rich smectite (Baldermann et al., 2015; Mackenzie & Garrels, 1966; Michalopoulos & Aller, 1995; Michalopoulos et al., 2000; Scholz, Severmann, McManus, Noffke, et al., 2014). The incorporation of Fe into authigenic silicates has been demonstrated to be particularly prevalent in tropical shelf environments such as the Amazon shelf (Michalopoulos & Aller, 1995; Michalopoulos et al., 2000; Spiegel et al., 2021) where reactive Fe oxide minerals originating from intense tropical weathering in the hinterland are particularly abundant (Michalopoulos & Aller, 2004). Conversion of reactive Fe oxide minerals to authigenic clay minerals may explain low proportions of reactive Fe in continental margin sediments compared to river suspended particles, as these clay minerals are not considered part of the reactive Fe or Fe_{HR} pools.

Even though clay minerals are generally not considered part of the highly reactive Fe pool, it is currently unknown if authigenic clay minerals are dissolved by the standardized sequential extraction scheme, which is widely applied to determine Fe_{HR} in marine sediments and to evaluate early diagenetic Fe cycling in modern marine sediments (e.g., Baldermann et al., 2015; Henkel et al., 2016; Lenstra et al., 2019; Scholz, Schmidt, et al., 2019) and paleo-redox conditions in the geological record (e.g., Poulton & Canfield, 2011; Poulton et al., 2010; Raiswell et al., 2018). In this study, we evaluate the impact of authigenic clay formation (i.e., reverse weathering) on sedimentary Fe speciation across the Amazon shelf, which is a well-known type locality for reverse weathering (Michalopoulos and Aller, 1995, 2004; Spiegel et al., 2021). We also test the hypothesis that reverse weathering may reduce the proportion of reactive Fe in continental margin sediments relative to river suspended particles.

2. Study Area

The Amazon River is characterized by high discharge rates of water and suspended sediment (annual discharge of 5,444 km^3 of water (Dai et al., 2009), containing $1{,}200 \cdot 10^{12}$ g of suspended sediment (Milliman and Sivitsky, 1992)). The majority of the particulate load discharged by the Amazon River originates from the Andes (Meade et al., 1985), whereas a minor fraction is derived from the tropical lowlands. Therefore, Amazon suspended sediments contain considerable amounts of primary silicate minerals (e.g., mica and chlorite) and soil-derived clay minerals (e.g., kaolinite and montmorillonite) (Gibbs, 1967). Previous studies reported particulate total Fe to aluminum ratios (Fe_T/Al) between 0.42 and 0.48 at different locations along the Amazon River and

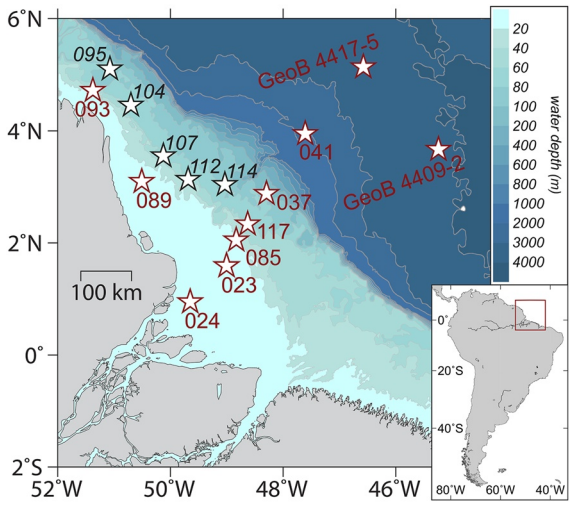

Figure 1. Bathymetric map of the study area showing the location of sediment (red stars) and suspended particulate matter (black stars) samples along an offshore and an along shore transect. Water depth is shown as a color scheme in steps of 20 m (0–100 m depth), 200 m (200–1,000 m depth) and 1,000 m (below 1,000 m depth).

on the Amazon shelf (Martin & Meybeck, 1979; Poulton & Raiswell, 2000; Sholkovitz & Price, 1980), which is similar to the Fe_T/Al of 0.44 of the average upper continental crust (Taylor & McLennan, 2009). Poulton and Raiswell (2002) reported an average reactive Fe to total Fe ratio of 0.47 for Amazon River particulates. Despite the low prevalence of highly weathered sediment sources for the Amazon River particulate load, this value is high in comparison to most other rivers in their data base, which indicates that Fe speciation is dominated by intensely weathered material from the Amazon lowlands.

The Amazon continental shelf is exposed to the North Brazil Current (NBC) with flow speeds of 40–80 cm s^{-1} across the shelf and strong tidal currents reaching up to 200 cm s^{-1} current speed (Candela et al., 1992; Nittrouer et al., 1986, 1995). The suspended sediment plume discharged by the Amazon River is advected toward the northwest by a combination of these forces and wind-induced surface waves (Kuehl et al., 1986; Nittrouer et al., 1986). High sedimentation and sediment mass accumulation rates prevail on the Amazon shelf (up to 10 cm yr^{-1} and 6.9 g cm^{-2} yr^{-1}, respectively) (Kuehl et al., 1986). The grain size of sediments deposited on the inner shelf (<70 m water depth) is primarily clayey silt or silty clay, while the outer shelf (70–100 m water depth) is characterized by a relict sand layer excavated by current erosion (Gibbs, 1973; Kuehl et al., 1986; Nittrouer et al., 1983). The highly dynamic current system on the Amazon shelf results in frequently occurring resuspension events, which continuously rework up to 150 cm of the upper sediment package (Kuehl et al., 1986).

3. Materials and Methods

3.1. Sample Collection and Pore Water Analyses

Sediment samples were collected during research cruise M147 RV Meteor (Koschinsky et al., 2018). This cruise to the discharge area of the Amazon River took place from late April to the end of May 2018 during the period of high riverine discharge. A multiple corer (MUC) was deployed at several stations across the Amazon shelf and slope. This study focuses on two transects comprising eight stations in total. One transect represents a section from the Amazon River mouth to the open ocean (offshore transect, stations 024, 023, 085, 117, 037, and 041; Figure 1) and another transect reflects a section parallel to the shore following the sediment plume toward the northwest (along shore transect, stations 023, 089, and 093; Figure 1). Suspended particulate matter in near-bottom water was collected near the along shore transect (Figure 1; Table 1). The particulate matter samples were obtained using a trace metal-clean CTD (station 095) or a single O.T.E. bottle on a wire (stations 104, 107, 112, 114). Additionally, solid phase sediment samples from two locations on the Amazon deep-sea fan were included in this study (GeoB 4417-5 and GeoB 4409-2 in Figure 1) to extend the offshore transect toward the open ocean. These samples were obtained with a gravity corer during RV Meteor cruise M38-2, which were subsampled with syringes at 5 cm depth intervals (Bleil et al., 1998).

The MUCs were sampled in a cool lab at 12°C at the shallower stations and 4°C at the deeper station 041 on board of the research vessel immediately after retrieval. The bottom water overlying the sediment within the core liners was sampled with a pre-cleaned (HCl) syringe and filtered through a pre-cleaned 0.2 µm polycarbonate (PC) syringe filter (stations 023 to 041) or a 0.2 µm cellulose acetate (CA) syringe filter (stations 085 to 117). Sediment cores were sub-sampled into pre-weighed plastic cups in intervals of 1 cm in the uppermost 6 cm and in intervals of 2 cm in the depth interval between 6 cm and the bottom of the cores. At six of the selected stations (024, 041, 085, 089, 093, and 117) a second sediment core from the same deployment was sampled for pore waters within a glove bag filled with nitrogen gas. The depth intervals were adjusted to visually distinguishable sediment layers (mainly based on sediment color), such that 12 samples were adequately spaced across the core length. The sediment was transferred into pre-cleaned 50 mL centrifuge tubes and centrifuged at 4°C or 12°C at 3,500 rpm for 40 min. Afterward, the centrifuge tubes were transferred to another nitrogen filled glove bag and pore water samples were filtered through pre-cleaned 0.2 µm PC syringe filters (stations 023 to 041) or 0.2 µm

Table 1
List of CTD, MUC and Gravity Core Stations Including Latitude, Longitude and Sampling Depth

Station	Device	Latitude	Longitude	Sampled depth (m)	Salinity (psu)	Temperature (°C)	Bottom water oxygen (μM)	TOC wt%
022	CTD	01°35,658′N	049°00,173′W	5	13.7	28.0	140	
023	MUC	01°35,653′N	049°00,195′W	16.3	–			0.45 ± 0.18
025	CTD	00°57,107′N	049°38,864′W	9	0.2	28.4	162	
024	MUC	00°57,108′N	049°38,864′W	22.1	0.2			0.58 ± 0.12
035	CTD	02°51,448′N	048°15,729′W	84	36.1	26.8	189	
037	MUC	02°52,849′N	048°17,665′W	102.1	–			0.04 ± 0.01
040	CTD	03°57,315′N	047°36,189′W	1,850	35.0	3.5	252	
041	MUC	03°56,933′N	047°36,313′W	1,974.2	34.6			0.41 ± 0.05
084	CTD	02°03,103′N	048°49,929′W	12	3.5	27.8	234	
085	MUC	02°03,053′N	048°49,926′W	24.9	35.3			0.57 ± 0.10
088	CTD	03°06,020′N	050°30,075′W	9	10.5	27.3	232	
089	MUC	03°05,657′N	050°30,464′W	21.1	28.0			0.65 ± 0.02
092	CTD	04°43,309′N	051°22,712′W	49	20.7	26.8	206	
093	MUC	04°43,150′N	051°22,514′W	50.6	36.6			0.65 ± 0.07
118	CTD	02°04,192′N	048°17,068′W	49	35.8	28.0	178	
117	MUC	02°19,249′N	048°37,903′W	53.7	37.4			0.54 ± 0.08
GeoB 4409-2		03°40.000′N	045°14.500′W	3,846				0.40 ± 0.08
GeoB 4417-5		05°08.300′N	046°34.500′W	3,511				0.46 ± 0.13

Note. For MUC and gravity core stations, sampling depth equals water depth. Salinity, temperature and bottom water oxygen as well as total organic carbon (TOC ± SD) data are presented, if available.

CA syringe filters (stations 085 to 117). The pore water samples were acidified to pH < 2 with HCl (sub-boiling distilled). All solid phase sediment and water samples were stored at 4°C for further analysis in the home laboratory after the cruise.

Pore water nitrate concentrations were measured on board within 24 hr after sampling with a SEAL QuAAtro continuous flow auto analyzer. The measurements were calibrated with an eight-point-calibration-curve, which was checked against reference materials for nutrient concentrations in seawater (CRM Lot. CG and CRM Lot. BW; see Table S1 in Supporting Information S1) before and after each run.

Depending on the concentration range, dissolved Fe was determined by inductively coupled plasma optical emission spectrometry (ICP-OES, Varian 720-ES) or mass spectrometry (ICP-MS, Agilent 7500). For correction of instrumental mass bias and signal drift, samples and standards were spiked with indium. Samples and standards were diluted with 3% HNO_3 and calibration standards were mixed with additional NaCl to be comparable to the sample matrix.

Upon recovery, the O.T.E. bottles for sampling of suspended particulate matter were carried into a trace metal clean sampling container. The water containing the suspended particulate material was directly filtered through acid washed 25 mm 0.2 μm polyethylene sulfone filters (Supor, Pall Gelman) by pressurizing the O.T.E. bottles (1.5 bar N_2). The filters were subsequently stored in the dark at −20°C.

3.2. Solid Phase Analyses

Sediment samples were weighed, freeze-dried and weighed again to determine water content and porosity. To determine total concentrations of Fe, aluminum (Al) and potassium (K), freeze-dried and ground sediment samples were completely digested following standard procedures (e.g., Scholz et al., 2011). In brief, 100 mg of sediment were digested in an acid mix consisting of 2 mL 40% HF, 2 mL 65% HNO_3 and 3 mL 60% $HClO_4$ at 185°C for 8 hr. Subsequently the acids were evaporated to dryness at 190°C and 1 mL of HNO_3 was added and

Table 2
Sequential Extraction Scheme for the Highly Reactive Fe Pool (Fe_{HR}) (Poulton & Canfield, 2005)

Fe fraction	Chemical extractant	Extraction time
Fe_{ac}	Sodium acetate (1 M)	48 hr at 50°C
Fe_{dith}	Sodium dithionite (50 g L^{-1})	2 hr
Fe_{oxal}	Ammonium oxalate (0.2 M) and oxalic acid (0.17 M)	6 hr

Note. Extractions were performed at room temperature if not stated otherwise.

evaporated again. The residue was re-dissolved in a mix of 1 mL 65% HNO_3 and 5 ml MilliQ water at 140°C. Finally, MilliQ water was added to the samples until a volume of 25 mL was reached.

A sequential extraction method was applied to determine operationally defined Fe fractions in Amazon shelf sediments. In the original studies on the reactive Fe content of river suspended particles and continental margin sediments, reactive Fe was defined based on a single-step sodium dithionite extraction (Poulton & Raiswell, 2002, 2005). To ensure comparability of our data to previously reported reactive Fe concentrations for river suspended particles (including those from the Amazon) and continental margin sediments with oxic bottom water, we also performed this single-step sodium dithionite extraction on Amazon shelf sediments (Canfield, 1989). In brief, 70 mg of freeze-dried sediment were treated with 10 mL of sodium dithionite solution (50 g L^{-1}) for 2 hr at room temperature in an overhead shaker (Raiswell et al., 1994). The solution was subsequently separated from the residue by centrifugation at 4,000 rpm for 4 min. By applying this method Fe oxide minerals are selectively dissolved and extracted but Fe carbonates or magnetite (Poulton & Canfield, 2005), which may form during early sediment diagenesis (Aller et al., 1986; Karlin et al., 1987; Vuillemin et al., 2019; Walker, 1984) are not quantitatively extracted. The results from the single-step sodium dithionite extraction will be abbreviated Fe_D in the following (accordingly, previously published ratios are referred to as Fe_D/Fe_T).

We further applied the multi-step Fe extraction scheme (Poulton & Canfield, 2005), which is more commonly applied in recent studies to evaluate early diagenetic Fe cycling and paleo-redox conditions in the geological record (e.g., Alcott et al., 2020; Henkel et al., 2016; Raiswell et al., 2018; Scholz, Schmidt, et al., 2019). This extraction scheme consists of three steps, which are summarized in Table 2. Upon completion of the extraction, the extraction solutions were separated from the residue by centrifugation at 4,000 rpm for 4 min. Recent studies (Hepburn et al., 2020; Slotznick et al., 2020) demonstrated that the mineral phases extracted by the individual steps differ considerably from those defined in the original study by Poulton and Canfield (2005). Therefore, we follow previous studies and denominate individual fractions according to the extraction chemicals rather than the originally intended target phases (Table 3) (Henkel et al., 2016). In the original study, the first extraction step was intended to dissolve crystalline Fe carbonates from ancient sedimentary rocks. For modern marine sediments, a more gentle 24 hr acetate extraction at room temperature was recommended instead (Poulton & Canfield, 2005). Recent studies have demonstrated that the 48 hr acetate step at 50°C can extract much but not all Fe carbonate and, in addition, leads to dissolution of some of the Fe oxides and possibly some Fe contained in clay minerals (e.g., nontronite) (Hepburn et al., 2020; Slotznick et al., 2020). Given that Fe carbonates are abundant on the Amazon shelf (Aller et al., 1986) and since we intended to obtain a maximum estimate of the reactive Fe abundance for comparison with paleoenvironmental studies, we decided to apply the 48 hr acetate extraction at 50°C. It needs to be kept in mind that some Fe oxide and Fe containing clay minerals may have been extracted during this step.

The element concentrations of the solutions obtained from the total digestion, the single-step sodium dithionite Fe extraction and the sequential Fe extraction methods were measured by ICP-OES (Varian ICP 720-ES). The certified reference standards MESS-3 and PACS-3 as well as our in-house standard OMZ-2 were used to determine the reproducibility and accuracy (total element concentrations) of these measurements (Table 4). The long-term laboratory averages for OMZ-2 were calibrated against the standards of Alcott et al. (2020).

Acid volatile sulfide (mainly Fe monosulfide, FeS) and pyrite were extracted from the sediment using the chromium reduction method (Canfield et al., 1986). In brief, 0.5 g of sediment were mixed with 8 mL of 6 M HCl to dissolve FeS. The gaseous H_2S released was precipitated in a bubble trap filled with 10 mL of 5% zinc acetate solution. Afterward, the residue was mixed with 15 mL of chromium (II) chloride solution and heated to 175°C for 1 hr to dissolve pyrite. The concentrations of pyrite (Fe_{py}; no AVS was detected throughout this study) within

Table 3
Abbreviation of Fe Fractions Used Within This Study in Comparison to Previous Studies

Method	Abbreviation	Chemical extractant (as used in this study)	Targeted phase	Previously used abbreviation
Single-step Fe_D extr.	Fe_D	Sodium dithionite	Ferric (oxyhydr)oxides (e.g. ferrihydrite, goethite)	Fe_{HR}[a]
	Fe_T	$HF\text{-}HClO_4\text{-}HNO_3$	Total Fe	Fe_T[a]
Seq. Fe extraction (sediment)	Fe_{ac}	Sodium acetate	Carbonate Fe, including siderite and ankerite	Fe_{carb}[b]
	Fe_{dith}	Sodium dithionite (seq. extr.)	Crystalline Fe oxides (e.g. goethite, hematite)	Fe_{ox2}[b]/Fe_{ox}[c]
	Fe_{oxal}	Ammonium oxalate and oxalic acid	Magnetite	Fe_{mag}[b,c]
	Fe_{py}	Chromium(II) chloride	Pyrite	Fe_{py}[b,c]
	Fe_{HR}	Sum of Fe_{ac}, Fe_{dith}, $Fe_{oxal,}$ and Fe_{py}		Fe_{HR}[b,c]
	Fe_T	$HF\text{-}HClO_4\text{-}HNO_3$	Total Fe	Fe_T[a]
Seq. Fe extraction (suspended particulate matter)	Fe_{HCl}	HCl	Poorly crystalline hydrous ferric oxides and particle-associated reduced Fe(II)	$Fe(III)_{HFO}$[c]/$Fe(II)_{red}$[c]
	Fe_{dith}	Sodium dithionite (seq. extr.)	Crystalline Fe oxides (e.g. goethite, hematite)	Fe_{ox2}[b]/Fe_{ox}[c]
	Fe_{oxal}	Ammonium oxalate and oxalic acid	Magnetite	Fe_{mag}[b,c]
	Fe_{HF}	HF	Fe silicates	Silicate[d]
	Fe_{HNO3}	HNO_3	Pyrite	Pyrite[d]
	Fe_{HR}	Sum of Fe_{HCl}, Fe_{dith}, Fe_{oxal} and Fe_{HNO3}		
	Fe_T	Sum of all fractions		

[a]Poulton and Raiswell (2002). [b]Poulton and Canfield (2005). [c]Zegeye et al. (2012). [d]Huerta-Diaz and Morse (1990).

the sediment can be calculated stoichiometrically from the amount of released S^{2-}, which was determined via photometric measurement of the amount of ZnS formed within the bubble trap. Following most studies on Fe speciation in modern and ancient marine sediment, individual Fe fractions (Fe_{ac}, Fe_{dith}, $Fe_{oxal,}$ and Fe_{py}) are summarized as Fe_{HR} and normalized concentrations that are based on the multi-step extraction are referred to as Fe_{HR}/Fe_T.

A combined version of the Fe extraction method described above and the ones published by Huerta-Diaz and Morse (1990) and Zegeye et al. (2012) was applied to determine Fe and Al concentrations as well as Fe speciation

Table 4
Analytical Results for Reference Materials Relative to Certified Values (if Available) or Long-Term Laboratory Averages for Sediment Analyses

		Al (mg/g)	FeT (mg/g)	FeT/Al	Number of. observations	Fe_{ac} (mg/g)	Fe_{dith} (mg/g)	Fe_{oxal} (mg/g)	Fe_{HR} (mg/g)
MESS-3	Certified	85.9 ± 2.3	43.4 ± 1.1	0.505					
	Measured[a]	82.2 ± 0.7	40.7 ± 0.3	0.496					
	Deviation	4.4%	6.2%	1.8%					
PACS-3	Certified	65.8 ± 1.7	41.1 ± 1.1	0.625					
	Lab. Avg.				20	5.2 ± 0.2	3.3 ± 0.2	2.7 ± 0.2	11.3 ± 0.6
	Measured[a]	61.6 ± 1.1	39.6 ± 1.6	0.643	4	5.3 ± 0.4	3.4 ± 0.2	2.6 ± 0.1	11.3 ± 0.6
	Deviation	6.4%	3.6%	2.9%		0.8%	2.8%	2.8%	0.3%
OMZ-2	Lab. Avg.	52.7 ± 0.4	23.1 ± 0.2	0.438	24	1.5 ± 0.1	2.5 ± 0.1	1.1 ± 0.1	5.1 ± 0.2
	Measured[a]	52.5 ± 0.8	22.7 ± 0.3	0.433	8	1.6 ± 0.1	2.5 ± 0.1	1.0 ± 0.1	5.1 ± 0.2
	Deviation	0.4%	1.6%	1.2%		1.4%	0.3%	5.2%	0.5%

[a]Results obtained within this study.

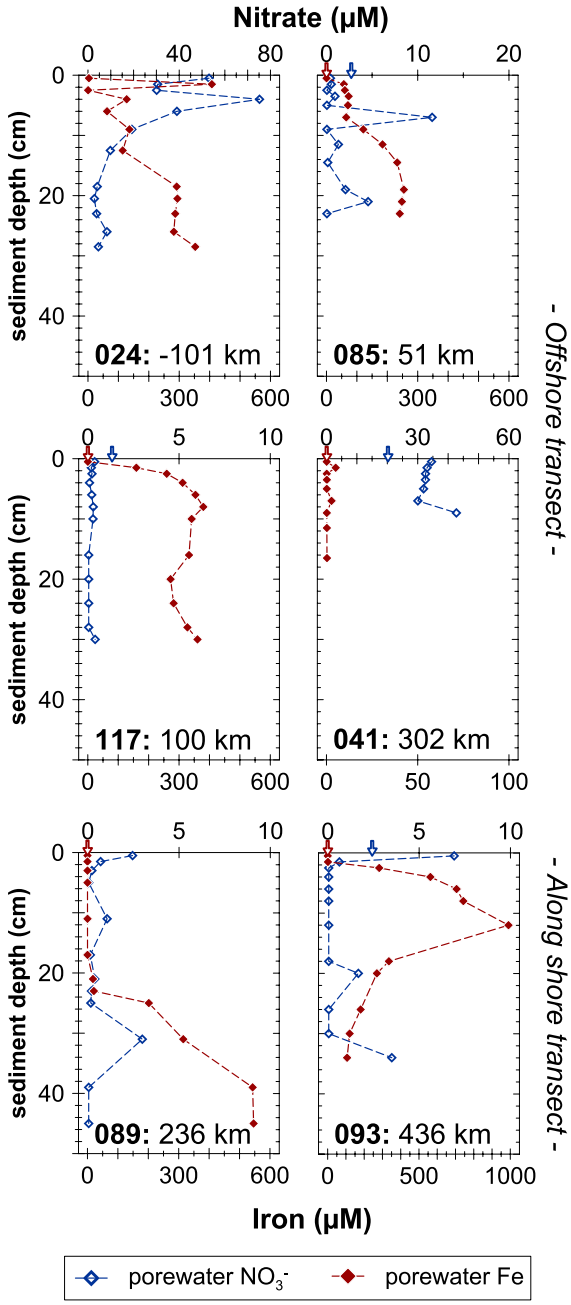

Figure 2. Pore water Fe and nitrate concentrations for stations 024, 085, 117, and 041 located on the offshore transect and stations 089 and 093 located on the alongshore transect. The distance from the intersection station 023 is noted behind the respective station number (station 024 has a negative distance as it is located shoreward of station 023). Vertical arrows at the top *x*-axes depict bottom water concentrations. Note differing *x*-axis scales. All presented data can be found in Table S2 in Supporting Information S1.

in the suspended particulate matter. Carbonate-associated Fe and poorly crystalline Fe oxides (ferrihydrite) were extracted with 2 mL 0.5 M HCl for 1 hr at room temperature (Fe_{HCl}). Crystalline Fe oxides (goethite and hematite) and magnetite were extracted as described above for Fe_{dith} and Fe_{oxal} except that only 2 mL of extractant were used. For the extraction of Fe silicates, the remaining residue was treated with 2 mL 10 M HF for 1 hr and after a first separation with another 2 mL 10 M HF for 16 hr. Afterward, 1 g of solid boric acid was added to the mixture to dissolve solid fluorides and the extraction was continued for 8 hr. After separation, the residue was washed with 2 mL boiling MilliQ. The solutions of these three steps (2 mL HF, 2 mL HF + boric acid, MilliQ wash) were combined and represent the silicate fraction (Fe_{HF}). Thereafter the residue was treated with 2 mL concentrated HNO_3 for 2 hr and washed with 2 mL pure water to extract pyrite (Fe_{HNO3}). The concentrations were measured by ICP-MS (Agilent Technologies 7500 Series). Using this method, Fe_T and Al were calculated as the sum of the Fe and Al in individual fractions. The combined fractions Fe_{HCl}, Fe_{dith}, $Fe_{oxal,}$ and Fe_{HNO3} represent the Fe_{HR} fraction within suspended particulate matter. An overview about the various sequential extraction schemes, calculation of Fe_{HR} for different sample types and abbreviations is given in Table 3.

For the determination of total organic carbon, freeze-dried sediment was weighed into a silver cup and carbonate carbon was removed via acidification with 0.25 N hydrochloric acid. The measurement was then performed via flash combustion in an Elemental Analyzer (Euro EA).

4. Results

4.1. Pore Water Data

Pore water Fe concentrations ranged from 0.06 to 990 µM (Figure 2). The lowest Fe concentrations were generally measured close to the sediment surface. In most of the analyzed sediment cores (stations 024, 085, 117, and 093) Fe concentrations increased with sediment depth within the first 2 cm and reached concentration maxima between 255 µM (085) and up to 990 µM (093). At station 089 the increase of dissolved Fe concentrations started at a depth of 20 cm and reached 546 µM at the bottom of the core. The pore water Fe profile at station 041 significantly differed from the others and was characterized by a narrow dissolved Fe peak of only 5 µM at 1.5 cm depth and low Fe concentrations in the rest of the core. At station 093 the dissolved Fe concentration decreased again below ~15 cm sediment depth. Iron concentrations within the uppermost pore water samples (0–1 cm) were similar to Fe concentrations in the overlying bottom water.

Pore water nitrate concentrations ranged from below 0.05–75.2 µM. At most of the stations, a peak of dissolved nitrate was observed above the Fe maximum. All sediment cores displayed additional maxima of dissolved nitrate in between or below peaks of high dissolved Fe concentrations.

4.2. Solid Phase Data

The total Fe content in the sediment solid phase (Fe_T) ranged from 0.9 wt% to 5.4 wt% (Figure 3). The downcore variability of Fe_T decreased from the stations close to the Amazon River mouth (024 and 023; 1.6, and 2.4 wt% Fe_T range) to the distal ends of the offshore and alongshore transects (GeoB 4417-5 and station 093; 0.5 and 0.4 wt% Fe_T range, respectively). The total Al content ranged from 1.6 wt% to 10.7 wt% with a variability similar to that of the total Fe content. Sedimentary K content ranged from 0.6 wt% to 2.4 wt% (Table S3 in Supporting Information S1).

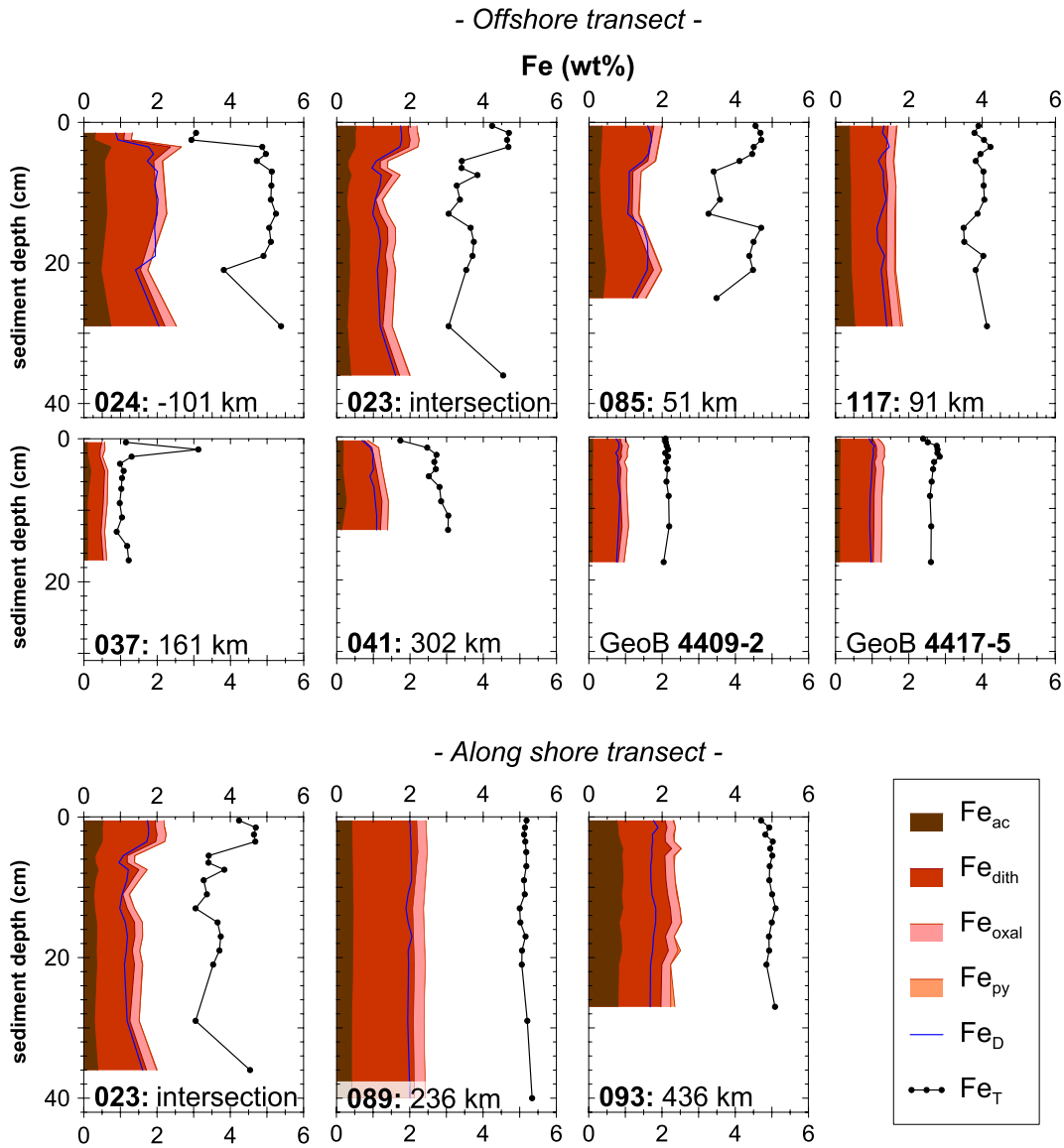

Figure 3. Concentration-depth profiles of Fe_{ac}, Fe_{dith}, Fe_{oxal}, and Fe_{py} of the cores of this study adding up to the combined concentration of highly reactive Fe (Fe_{HR}). Fe_D and Fe_T are shown as a solid blue and a solid back line, respectively. The distance from the intersection station 023 is noted behind the respective station number. All presented data can be found in Table S3 in Supporting Information S1.

The Fe_T/Al of sediment samples from most of the sediment cores ranged from 0.47 to 0.56 (mean of 0.50 ± 0.02) (Figure 4). Samples from station 037 exceeded these values reaching Fe_T/Al of up to 1.93. All analyzed samples exceeded the Fe/Al signature of average upper continental crust (0.44; Taylor & McLennan, 2009) but were generally consistent with the range of Fe_T/Al previously reported for Amazon River suspended sediment (0.46; Poulton & Raiswell, 2002, 0.47; Martin & Meybeck, 1979). Apart from station 037, Fe_T/Al values were approximately constant across the entire Amazon continental margin and no spatial trend of enrichment or depletion was identified (Figure 4). The sedimentary K/Al of most of the Amazon shelf sediment samples ranged from 0.22 to 0.30 (mean of 0.24 ± 0.02) (Figure 4). Only samples from station 037 exceeded this range with K/Al ranging from 0.38 to 0.47. All analyzed sediment samples exceeded the K/Al ratio of Amazon River suspended sediment (0.16; Martin and Meybeck (1979)).

The sediments of station 037 differed from the other stations in that they were characterized by exceptionally low Fe_T concentrations but higher Fe_T/Al and K/Al compared to all other stations and Amazon River suspended

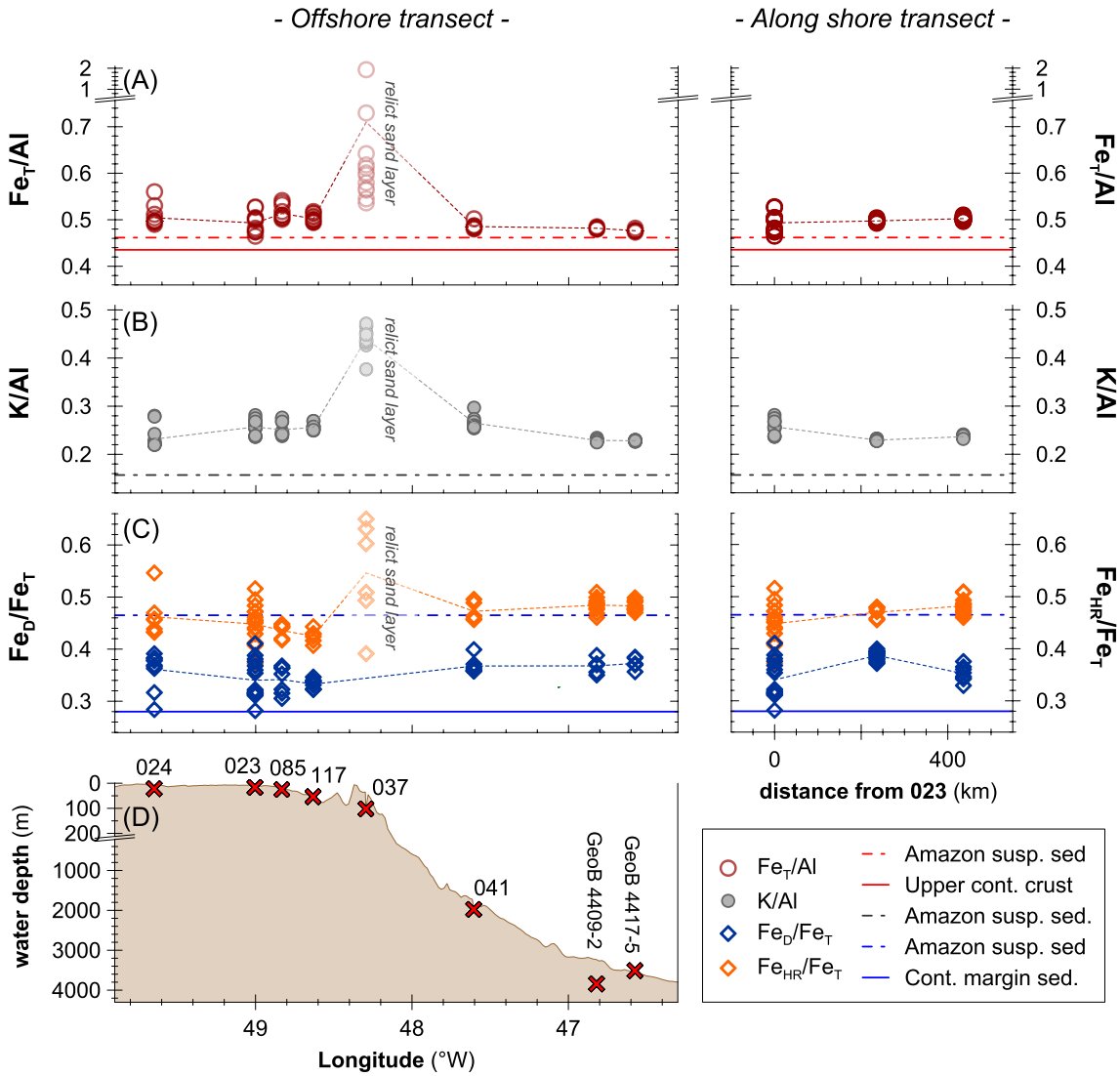

Figure 4. Sediments geochemistry data along the offshore and along shore transects: (a) Solid phase Fe_T/Al, (b) K/Al and (c) Fe_D/Fe_T and Fe_{HR}/Fe_T. Dashed lines depict the Fe_T/Al, K/Al, and Fe_D/Fe_T of Amazon suspended sediments (Martin & Meybeck, 1979; Poulton & Raiswell, 2002). Solid lines depict the Fe_T/Al of upper continental crust (Taylor & McLennan, 2009) and the Fe_D/Fe_T of average continental margin sediments with oxic bottom waters (Poulton & Raiswell, 2002). The bathymetry along the offshore transect and location of sediment core stations is shown in (d). Note that core GeoB 4409-2 is projected onto the offshore transect; its actual location is further southwest (see Figure 1). All presented data can be found in Table S3 in Supporting Information S1.

sediment. This station was located within a belt of sandy sediments on the outer Amazon shelf, which was previously reported to represent a relict sand layer meaning that the material does not correspond to the fine-grained suspended material discharged by the modern Amazon River (Adams et al., 1986; Kuehl et al., 1986; Milliman and Barretto, 1975). Therefore, samples of station 037 will not be further considered in the discussion.

Reactive Fe recovered from sediment samples by the single-step sodium dithionite extraction (Fe_D) ranged from 0.69 to 2.06 wt% (Figure 3). The proportion of Fe_D in the total Fe pool ranges from 0.28 to 0.41 (0.36 ± 0.03 on average), which is about 22% lower than the Fe_D/Fe_T of Amazon suspended sediment of 0.47 reported by Poulton and Raiswell (2002). Within the individual fractions of the multi-step sequential extraction (Figure 3), the sodium dithionite extractable Fe (Fe_{dith}) was the largest fraction reaching concentrations ranging from 0.37 to 1.79 wt% representing 49.7%–73.9% of the combined Fe_{HR} fraction. The sodium acetate extractable Fe (Fe_{ac}) concentrations ranged from 0.09 to 0.74 wt% representing a share of 9.4%–29.1% of the Fe_{HR} fraction. The ammonium oxalate and oxalic acid extractable Fe concentrations (Fe_{oxal}) ranged from 0.08 to 0.31 wt% representing a share of 9.4%–17.4% of the Fe_{HR}-phases. Only the deepest samples of stations 093 and 117 showed measur-

able concentrations of Fe_{py}. In these samples the concentrations ranged between 0.03 and 0.12 wt% representing a share of 1.9%–4.9% of the Fe_{HR}-fraction. Variations in the total Fe concentrations (Fe_T) within the analyzed sediment cores can mainly be attributed to concentration changes within the Fe_{HR} fractions, especially the Fe_{dith} and the Fe_{ac} fractions. The sum of Fe_{ac} and Fe_{dith} was similar to Fe_D and also the downcore variability of the sum of Fe_{ac} and Fe_{dith} was similar to Fe_D.

Combining all the reactive Fe concentrations obtained by the multi-step sequential extraction yields Fe_{HR} from 0.85 to 2.66 wt%, which is about 23% higher than sedimentary Fe_D. The Fe_{HR}/Fe_T of Amazon shelf sediments ranges from 0.37 to 0.55 with a mean of 0.47 ± 0.03). This mean value is equal to the Fe_D/Fe_T of Amazon River suspended sediment (Poulton & Raiswell, 2002). The Fe_{HR}/Fe_T of Amazon shelf, slope and deep-sea fan sediments were all higher than the Fe_D/Fe_T of average continental margin sediment underlying oxic bottom water of 0.28 ± 0.06 (Poulton & Raiswell, 2002). Across the entire Amazon continental shelf (excluding station 037), Fe_{HR}/Fe_T remained close to the average and no spatial trend was observed (Figure 4).

The suspended particulate matter sampled at the water column stations near the along shore transect was characterized by Fe_T/Al of 0.72–0.89 (Table S4 in Supporting Information S1). These Fe_T/Al ratios of outer shelf suspended particles were higher than previously reported Fe_T/Al for Amazon estuary and inner shelf suspended matter (0.42 ± 0.04 and 0.46 ± 0.05; Sholkovitz & Price, 1980). The Fe_{HR}/Fe_T of the suspended particulate matter samples ranged from 0.70 to 0.76.

5. Discussion

5.1. Early Diagenesis Across the Amazon Shelf

Consistent with previous studies (Aller et al., 1986, 2004), high pore water Fe concentrations were found in most of the pore water samples analyzed in this study (Figure 2). This observation along with low concentrations of solid phase Fe sulfide (Figure 3) implies that biogeochemical cycling within Amazon shelf sediments is dominated by Fe reduction whereas net sulfate reduction and burial of reduced sulfur are only of subordinate importance (Aller & Blair, 1996; Aller et al., 2004, 2010). Sedimentary organic carbon concentrations on the Amazon shelf (Table 1) are theoretically high enough to fuel intense organic carbon degradation by sulfate reduction (e.g., Arndt et al., 2013; Jorgensen, 1982) leading to Fe sulfide precipitation. The predominance of Fe-rich (i.e., ferruginous) conditions in pore water despite relatively high organic carbon concentrations can be explained by high solid phase Fe concentrations and, more importantly, frequently occurring remobilization of the uppermost sediment package. During such resuspension events the diagenetic sequence is reset by re-oxidation of hydrogen sulfide to sulfate coupled to Fe reduction thus contributing to the maintenance of extensive Fe-rich zones in the pore water (Aller et al., 1986, 2010). The mixing and homogenization of the uppermost sediment package (up to 150 cm) (Aller et al., 2004; Kuehl et al., 1986) by resuspension and deposition events are also reflected by the pore water Fe and nitrate profiles observed in this study. Nitrogenous conditions (presence of nitrate but no oxygen, Fe and hydrogen sulfide) (Canfield & Thamdrup, 2009) are generally expected to be present at the sediment surface above the ferruginous zone (Froelich et al., 1979). The occurrence of multiple nitrogenous zones above, within and/or below ferruginous zones (stations 024, 085, 089 and 093 in Figure 2) is likely a transient feature related to previous resuspension events.

No significant gradient of dissolved Fe concentrations between the bottom waters and uppermost pore water samples was observed at any of the study sites. Consequently, and as expected in an area with a fully oxygenated water column (Table 1), a diffusive flux of dissolved Fe across the sediment-water interface can be excluded. Pore water Fe profiles indicate that dissolved Fe transported upwards by diffusion is reprecipitated at the sediment surface. It is possible that resuspension of the upper sediment parcel mobilizes Fe-rich particles and/or pore water dissolved Fe into the oxic water column. Furthermore, macrofauna could potentially transfer dissolved Fe across the sediment-water boundary despite oxic conditions at the sediment surface (Severmann et al., 2010). Such a mechanism could be facilitated by complexation of dissolved Fe by organic ligands or through formation of colloids (Homoky et al., 2011, 2021). Consistent with all of these mechanisms of Fe remobilization, suspended particulate matter samples from the outer Amazon shelf are characterized by elevated Fe_{HR}/Fe_T in comparison to shelf sediments. However, only a small number of suspended particulate matter samples were analyzed within this study. Thus, the overall importance of these processes cannot be quantified.

5.2. Diagenetic Redistribution Within the Reactive Iron Pool

The Fe within Amazon shelf sediments originates from suspended particles and dissolved Fe discharged by the Amazon River. Given that Fe is more mobile than Al in ferruginous pore waters, any loss or gain of Fe relative to these sources can be evaluated based on Fe_T/Al ratios. Previously reported Fe_T/Al ratios for Amazon suspended particles varied considerably, presumably due to differing sampling times and locations. Poulton and Raiswell (2000) reported an Fe_T/Al of 0.46 for Amazon River suspended sediment whereas Martin and Meybeck (1979) reported a slightly higher Fe_T/Al of 0.48. Gaillardet et al. (1997) reported significantly higher Fe concentrations within suspended particles of the Amazon River than the two afore mentioned studies, which could imply higher Fe_T/Al. However, no Al data were published in this study so that Fe_T/Al cannot be calculated.

In order to compare Fe_T/Al ratios of Amazon shelf sediments to the ratios of riverine suspended particles, the potential impact of dissolved Fe precipitation within the estuarine salinity gradient needs to be considered. The annual discharge of dissolved Fe ($F_{Fe,diss}$) from the Amazon River can be calculated as follows:

$$F_{Fe,diss} = [Fe]_{diss,river} \cdot m_{Fe} \cdot F_{H_2O,river} \quad (1)$$

where $F_{H_2O,river}$ refers to the annual discharge of water from the Amazon River (5,444 $km^3\ yr^{-1} = 5.44 \cdot 10^{15}$ L yr^{-1}; Dai et al., 2009) and m_{Fe} is the molecular mass of Fe (55.9 g mol^{-1}). The reported concentration of dissolved Fe within the Amazon River water ($[Fe]_{diss,river}$) varied in previous studies (e.g., Aucour et al. (2003): 1.8 μM; Bergquist and Boyle (2006): 2.5 μM). The resulting calculated annual discharge of dissolved Fe ($F_{Fe,diss} = 0.55 \cdot 10^{12}$ and $0.76 \cdot 10^{12}$ g yr^{-1} for 1.8 and 2.5 μM, respectively) can be compared to the annual discharge of solid phase Al and Fe.

The annual discharge of solid phase Al from Amazon River suspended particles ($F_{Al,part}$) is the product of the annual discharge of suspended sediment of the Amazon River ($F_{part} = 1{,}200 \cdot 10^{12}$ g yr^{-1}; Milliman & Syvitski, 1992) and the concentration of the Al within the suspended particles ($[Al]_{part}$ = 121.1 mg/g or 115 mg/g; Poulton & Raiswell, 2000 and Martin & Meybeck, 1979, respectively):

$$F_{Al,part} = F_{part} \cdot [Al]_{part} \quad (2)$$

This calculation yields a $F_{Al,part}$ of 145 10^{12} g yr^{-1} (using $[Al]_{part}$ from Poulton & Raiswell, 2000) or $138 \cdot 10^{12}$ g yr^{-1} (using $[Al]_{part}$ from Martin & Meybeck, 1979). An annual discharge of solid phase Fe within riverine suspended particles ($F_{Fe,part}$) of $67 \cdot 10^{12}$ g yr^{-1} and $66 \cdot 10^{12}$ g yr^{-1}can be calculated by analogy to $F_{Al,part}$ (Equation 2), that is, by using $[Fe]_{part}$ instead of $[Al]_{part}$ ($[Fe]_{part}$ = 55.9 mg/g (Poulton & Raiswell, 2000) or 55 mg/g (Martin & Meybeck, 1979)). By summing up the total Fe discharged by the Amazon River via suspended particles and dissolved Fe, an expected Fe_T/Al ratio of the Amazon shelf sediments can be calculated ($(Fe_T/Al)_{sed,exp}$):

$$\left(\frac{Fe_T}{Al}\right)_{sed,exp} = \frac{\left(F_{Fe,part} + F_{Fe,diss}\right)}{F_{Al,part}} \quad (3)$$

Based on this calculation, the expected Fe_T/Al of Amazon shelf sediments ranges from 0.47 to 0.49, which is within error of the observed Fe_T/Al of 0.50 ± 0.02. The above calculations are associated with a large uncertainty. Particulate Fe concentrations within the lower reaches of the Amazon River might be higher (Gaillardet et al., 1997) than those published by Poulton and Raiswell (2000) and Martin and Meybeck (1979), which may imply a higher Fe_T/Al in discharged particles. On the other hand, our calculation neglects any Al precipitation within the estuarine salinity gradient. Previous studies have shown that dissolved Fe and Al removal may be mediated by a different set of processes within different areas of the estuarine system (Mackin & Aller, 1984; Takayanagi & Gobeil, 2000). Furthermore, this decoupling continues on the shelf where sediments may represent a source or a sink for dissolved Al, depending on riverine discharge, bottom water turbulence and, thus, sediment resuspension dynamics (Mackin & Aller, 1984). Considering these uncertainties, we assume that the Fe_T/Al of Amazon shelf sediments is largely consistent with the composition of the source material indicating little net gain or loss of Fe from the sediment relative to river-derived particles.

The Fe_D/Fe_T of Amazon shelf sediments observed in this study (0.36 ± 0.03) is lower than the average Fe_D/Fe_T ratio reported for Amazon River suspended particles (0.47; Poulton & Raiswell, 2002). In contrast, the Fe_{HR}/Fe_T of 0.47 ± 0.03 obtained by the sequential extraction is similar to the Fe_D/Fe_T of riverine suspended particles (Figure 4). In general, reactive Fe within river suspended particles comprises Fe oxide minerals, which

are contained in the Fe_D fraction (Poulton & Raiswell, 2002). In contrast, within marine sediments Fe oxide minerals may be reductively dissolved and the dissolved Fe released may either be lost across the sediment-water interface or be re-precipitated as authigenic Fe carbonate, sulfide and silicate minerals (e.g., Aller et al., 1986; Canfield, 1989; Scholz, Severmann, McManus, Noffke, et al., 2014). These authigenic mineral phases are not extracted by a simple dithionite leach. However, they are at least partly recovered by the more elaborated Fe extraction scheme yielding Fe_{HR} (Poulton & Canfield, 2005). The mismatch in Fe_D/Fe_T between Amazon shelf sediments and river suspended particles but close similarity of Fe_{HR}/Fe_T of shelf sediments and Fe_D/Fe_T of river suspended particles are therefore indicative of an internal redistribution of Fe within the Fe_{HR} pool on the Amazon shelf.

5.3. Impact of Authigenic Mineral Formation on Sedimentary Iron Speciation

Pyrite concentrations in Amazon shelf sediments are generally too low to explain the mismatch between Fe_D/Fe_T and Fe_{HR}/Fe_T (Figure 3). However, the Fe_{dith} extraction step dissolved roughly 20% less Fe than the single-step dithionite extraction (Fe_D) within the Amazon shelf sediments. This observation indicates that a fraction of Fe_D was already dissolved by the Fe_{ac} extraction step, which was originally intended to recover Fe contained in carbonates (Poulton & Canfield, 2005). Recent studies revealed that the Fe_{ac} extraction can also partly dissolve Fe oxide minerals (e.g., hematite) and even Fe-containing clay minerals such as nontronite (Hepburn et al., 2020; Slotznick et al., 2020). The formation of nontronite can occur within Fe-reducing sediments and is potentially mediated by microbial extracellular polymeric substances (Harder, 1976; Ueshima & Tazaki, 2001). The redistribution of riverine Fe_D to sedimentary Fe_{ac} is thus not only due to the formation of authigenic Fe carbonates, but can also be related to the extraction of Fe from hematite and/or clay minerals such as nontronite. Geochemical evidence for the formation of such clay minerals within Amazon shelf sediments has previously been presented based on the same sample set as analyzed within this study. Spiegel et al. (2021) reported pore water profiles that are indicative of coincident removal of dissolved silica and potassium (K), which is consistent with the formation of authigenic silicate minerals via reverse weathering. Spiegel et al. (2021) also reported elevated sedimentary K/Al across the entire Amazon shelf (redrawn in Figure 4b) and quantified sedimentary K uptake by multiplying excess K relative to Amazon River suspended material by the annual discharge of particulate material. Their findings are consistent with early studies of reverse weathering and sedimentary K uptake in the study area (e.g., Michalopoulos & Aller, 1995, 2004; Michalopoulos et al., 2000).

Michalopoulos and Aller (1995) determined an average stoichiometry of Fe to K ($(Fe/K)_{clay}$) of 0.94 within clay minerals formed by reverse weathering on the Amazon shelf. We can utilize this value to evaluate the potential impact of authigenic silicate formation on sedimentary Fe speciation. To this end, sedimentary K uptake will be compared to the deficiency of sedimentary Fe_D on the Amazon shelf relative to riverine suspended Fe_D.

As a first step, the solid phase K data produced for our sediment samples were corrected for pore water K concentrations given that K dissolved in pore water was transferred to the solid phase during the freeze-drying procedure (see Section 3.2). The K concentration within the wet sediment ($K_{T,wet}$) was calculated from the K concentrations of the freeze-dried sediment ($K_{T,dry}$) and the determined water content (u):

$$K_{T,wet} = K_{T,dry} \cdot (1 - u) \tag{4}$$

The mass of pore water dissolved K within the total wet sediment sample ($K_{pw,wet}$) was calculated from the pore water K concentration (K_{pw}) and the water content (u):

$$K_{pw,wet} = K_{pw} \cdot u \tag{5}$$

The corrected sedimentary K concentrations for the dry sediment samples ($K_{sed,dry}$) was then calculated from the difference of these two values divided by the relative amount of solid phase within the wet sediment ($1-u$):

$$K_{sed,dry} = \frac{K_{T,wet} - K_{pw,wet}}{1 - u} \tag{6}$$

Corrected solid phase K concentrations were on average 1.8% lower than uncorrected concentrations. The correction for station 023 was based on averaged pore water concentrations from station 089, as no original data was available for this station and bottom waters at station 023 and 089 had a similar salinity (see Table 1). Sedimentary

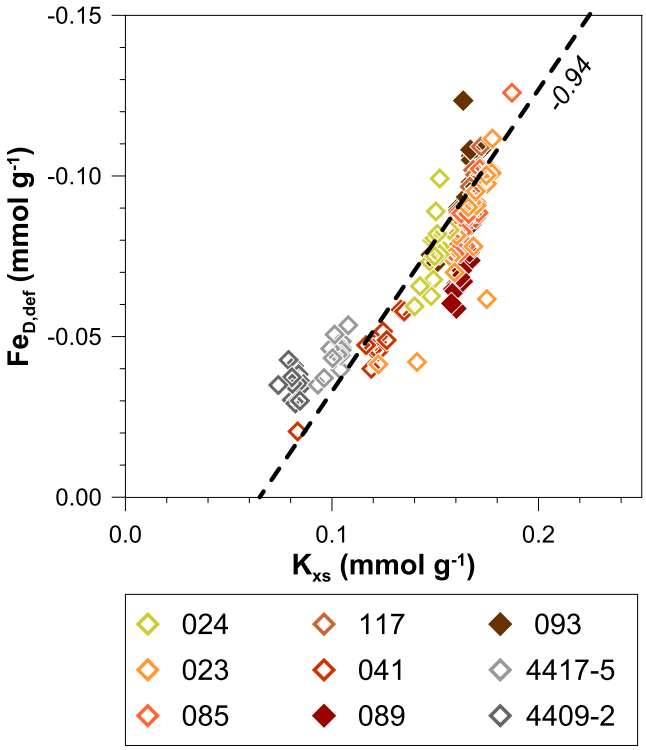

Figure 5. Plot of $Fe_{D,def}$ versus K_{xs} for all sediment samples. The individual stations are differentiated by color. The slope of the dashed line corresponds to the Fe:K stoichiometry of authigenic clay minerals forming by reverse weathering on the Amazon shelf (0.94; Michalopoulos & Aller, 1995). All presented data can be found in Tables S3 and S5 in Supporting Information S1.

K concentrations of samples from the Amazon deep-sea fan (GeoB 4417-5 and GeoB 4409) could not be corrected because no water content data were available.

Following the pore water K correction, the solid phase K data were corrected for the cation exchange capacity (CeC) of Amazon suspended sediments. It was previously demonstrated that Amazon suspended particles take up K upon contact with seawater (Sayles & Mangelsdorf, 1979). As it is not known whether this loosely adsorbed K is incorporated into minerals on the Amazon shelf, we subtracted it from the solid phase K concentrations using a mean CeC of K of 2.0 Δmeq/100 g (Sayles & Mangelsdorf, 1979). The CeC-corrected data were between 3% and 9% lower than the solid phase *K* data that were only corrected for pore water K (4% lower on average).

The sedimentary K uptake (K_{xs}, in mmol g^{-1}) was calculated applying the corrected K data (K_{corr}) and the K to Al ratio of riverine particulate matter ($(K/Al)_{part}$):

$$K_{xs} = \frac{\left(K_{corr} - \left(\frac{K}{Al}\right)_{part} \cdot Al_{sed}\right)}{m_K} \quad (7)$$

The $(K/Al)_{part}$ was calculated from data given by Martin and Meybeck (1979) (Al_{part} = 115 mg/g, K_{part} = 18 mg/g, i.e., $(K/Al)_{part}$ = 0.157) and m_K is 39.1 g/mol. Data for K_{corr} and Al_{sed} were obtained within this study (Al was not corrected for pore water concentrations, as these are neglectable low).

The deficiency of sedimentary Fe_D on the Amazon shelf relative to river suspended sediment ($Fe_{D,def}$, in mmol g^{-1}) can be calculated from the sedimentary Fe_D and Fe_T concentrations as well as the Fe_D to Fe_T ratio within riverine particulate matter ($(Fe_D/Fe_T)_{part}$):

$$Fe_{D,def} = \frac{\left(Fe_{D,sed} - \left(\frac{Fe_D}{Fe_T}\right)_{part} \cdot Fe_T\right)}{m_{Fe}} \quad (8)$$

The $(Fe_D/Fe_T)_{part}$ was taken from Poulton and Raiswell (2002; = 0.47) and m_{Fe} is 55.9 g/mol. Concentrations of Fe_D and Fe_T were obtained within this study (not corrected for pore water concentrations because pore water Fe concentrations are negligible).

A plot of the calculated $Fe_{D,def}$ versus K_{xs} data is shown in Figure 5. The $Fe_{D,def}$ and K_{xs} of sediments from the Amazon shelf, slope and deep-sea fan are generally consistent with a slope of −0.94. Thus, the ratio of Fe_D loss to K uptake is close to the Fe/K stoichiometry of authigenic clay minerals formed via reverse weathering (0.94; Michalopoulos & Aller, 1995). This observation highlights the importance of reverse weathering for the partitioning of sedimentary reactive species on the Amazon shelf. Furthermore, the observation of a relatively constant ratio of $Fe_{D,def}$ to K_{xs} across the Amazon shelf indicates that authigenic Fe-rich clay minerals are relative evenly distributed across the entire shelf, probably due to continuous sediment resuspension and transport by tidal currents.

The formation of authigenic Fe carbonate minerals such as siderite ($FeCO_3$) within the ferruginous Amazon shelf sediments was previously demonstrated based on pore water saturation state calculations and Scanning Electron Microscopy (SEM) (Aller et al., 1986). More recent studies in modern ferruginous sediments demonstrated that authigenic siderite forms as a result of organic carbon degradation and the accumulation of dissolved inorganic carbon in pore waters in the absence of H_2S (Vuillemin et al., 2019). Thus, authigenic carbonate formation is likely to contribute to the redistribution of Fe_D to Fe_{ac} within Amazon shelf sediments. Precipitation of authigenic carbonate and silicate minerals cannot be clearly distinguished based on the extraction method utilized within this study. However, considering the close correlation between Fe_D loss and K uptake (Figure 5), the formation

of authigenic clay minerals appears to be dominant for the redistribution of riverine Fe_D to Fe_{ac} within Amazon shelf sediments.

Since Fe_{ac} and Fe_{dith} cannot account for the entire riverine Fe_D pool, a fraction of riverine Fe_D must also be transferred to the Fe_{oxal} pool (originally meant to represent magnetite; Poulton & Raiswell, 2005) within the Amazon shelf sediments. The formation of authigenic magnetite in marine sediments has for example, been attributed to extracellular production by iron-reducing bacteria within ferruginous sediments, intracellular production by magnetotactic bacteria in the nitrogenous-ferruginous transition zone and potentially Fe^{2+}-oxidizing bacteria within the nitrogenous zone (Roberts, 2015). Therefore, a redistribution of river-derived Fe to the sedimentary Fe_{oxal} fraction seems plausible in the extended ferruginous zones of Amazon shelf sediments. Additionally, recent studies demonstrated that the Fe_{oxal} extraction step can also dissolve Fe silicate minerals such as berthierine or chamosite and nontronite (Hepburn et al., 2020; Slotznick et al., 2020). Chamosite and glauconite (which is a precursor of berthierine) may be formed authigenically in continental shelf sediments (Baldermann et al., 2015, 2022; van Houten and Purucker, 1984). Thus, the formation of authigenic Fe bearing silicate minerals discussed above likely contributed to the transfer of Fe_D to Fe_{oxal}.

6. Summary and Implications

The Amazon River is the world's largest river system draining an intensely weathered tropical terrain. Consequently, Amazon River suspended sediments are characterized by relatively high reactive Fe concentrations and Fe_D/Fe_T. In the Amazon shelf sediments, Fe_D/Fe_T ratios are diminished compared to the riverine suspended source material. In contrast, the Fe_{HR}/Fe_T of sediments on the Amazon shelf and deep-sea fan are identical to the Fe_D/Fe_T of Amazon suspended particles. The ratio of Fe_D loss to K gain in Amazon shelf sediments is similar to the Fe/K stoichiometry of authigenic Fe silicate minerals formed during reverse weathering on the Amazon shelf. Overall, our data are consistent with a scenario in which river-derived Fe oxides are converted to authigenic Fe silicate and carbonate minerals during early diagenesis. The conversion of Fe oxides to Fe silicate and carbonate minerals can explain the mismatch in Fe_D/Fe_T between Amazon shelf sediments and Amazon River suspended particles. Further research on the formation of Fe-rich silicate minerals at the land-ocean interface is required to evaluate the global relevance of reverse weathering processes as a sink for land-derived Fe oxides. The sequential extraction scheme by Poulton and Canfield (2005) has to be applied with caution in this context since an important fraction of the silicate-bound Fe is likely contained in the Fe_{ac} and Fe_{oxal} fractions of the Fe_{HR} pool.

The original definition of reactive Fe (Berner, 1970, 1984; Canfield, 1989; Poulton & Canfield, 2011) focused on the reactivity of Fe minerals with respect to hydrogen sulfide on early diagenetic timescales. The commonly applied sequential extraction method to determine the highly reactive Fe content of marine sediments explicitly includes sulfide minerals formed from reactive Fe oxides in the water column or during early diagenesis (Poulton & Canfield, 2005). Authigenic silicate minerals are also formed from reactive Fe oxides during early diagenesis. According to our findings and those of previous studies, authigenic silicate minerals are at least partly recovered by the multi-step sequential extraction scheme for the recovery of the Fe_{HR} pool (Hepburn et al., 2020; Slotznick et al., 2020). Furthermore, a number of recent studies have demonstrated that Fe-containing clay minerals may be dissolved, converted or precipitated by dissimilatory Fe reduction, pyrite formation, weathering and reverse weathering during early diagenesis (e.g., Baldermann et al., 2015, 2022; Eroglu et al., 2021; Laufer-Meiser et al., 2021; Scholz, Schmidt, et al., 2019; Scholz, Severmann, McManus, Noffke, et al., 2014; Vorhies & Gaines, 2009). We therefore argue that the conventional separation of classic reactive Fe minerals (Fe oxides, carbonates, and sulfides) from allegedly unreactive Fe-containing clay minerals needs to be reconsidered. Depending on the scientific perspective of the respective study, it might be meaningful to broaden the term "reactive Fe." For example, if one is interested in the total amount of biogeochemically reactive Fe at the time of deposition (e.g., in paleo-environmental studies), it might be useful to explicitly include authigenic silicate minerals. Furthermore, if reductive remobilization of Fe oxides or the role of Fe oxides in organic matter preservation is concerned, it may be necessary to consider the impact of reverse weathering on Fe oxide concentrations. The role of authigenic silicate minerals in organic carbon preservation should be investigated in future studies.

Our findings have further implications for the use of sedimentary Fe speciation as a paleo-redox proxy. The commonly applied sedimentary Fe_{HR}/Fe_T threshold for water column anoxia of 0.38 (Poulton & Canfield, 2011) was originally based on a single-step sodium dithionite leach (Raiswell & Canfield, 1998). Amazon shelf sediments are characterized by Fe_D/Fe_T below this threshold. In contrast, Fe_{HR}/Fe_T in these sediments clearly exceeds

the threshold for anoxia despite well-oxygenated conditions in the overlying water column. The offset between Fe_D/Fe_T and Fe_{HR}/Fe_T may be explained by the different minerals recovered with the Fe_D (Fe oxides) and the Fe_{HR} (Fe oxides, carbonates and silicates) pools. A similar observation was made by Wei et al. (2021) on sediments originating from the subtropical mountainous island of Hainan in the northern South China Sea. These authors reported an offset between Fe_{HR}/Fe_T and Fe_D/Fe_T similar to that observed on the Amazon shelf in our study. We therefore argue that applying the anoxia threshold, which was originally defined based on a single step sodium dithionite leach as part of Fe speciation data that were generated applying the multi-step sequential extraction scheme, may result in misleading interpretations.

The Fe_{HR}/Fe_T of Amazon shelf sediments is higher than the Fe_D/Fe_T of average continental margin sediments but essentially identical to the Fe_D/Fe_T of Amazon river suspended particles (Poulton & Raiswell, 2002). Such elevated reactive Fe to total Fe ratios of river suspended particles represent a terrestrial signal related to high continental runoff and intense chemical weathering (Canfield, 1997; Poulton & Raiswell, 2002). On the Amazon shelf, this terrestrial signal in the Fe_{HR}/Fe_T data remains unaltered across the shelf, slope and deep-sea fan. We therefore suggest that sedimentary Fe_{HR}/Fe_T data may not strictly reflect redox conditions in the ocean but may also provide information about the terrestrial supply of reactive Fe as a function of chemical weathering and continental runoff. Past periods of global warming were often accompanied by intensified chemical weathering on land (e.g., the Late Permian (e.g., Cao et al., 2019; Sun et al., 2018) and Late Cretaceous (e.g., Föllmi, 1995; Pogge von Strandmann et al., 2013)), which likely increased terrestrial Fe oxide supply and contributed to elevated sedimentary Fe_{HR}/Fe_T during those times (Scholz, 2018; Scholz, Beil, et al., 2019). Furthermore, an increased terrestrial supply of Fe oxides may have amplified organic carbon preservation and burial during greenhouse episodes (Kennedy & Wagner, 2011). Importantly, we do not intend to negate the utility of Fe_{HR}/Fe_T as a marine paleo-redox indicator. Instead, we argue that considering the potential control of riverine Fe oxide supply and reverse weathering on sedimentary Fe speciation may provide additional information on paleo-environmental conditions.

Data Availability Statement

The figures in this paper were made with version 10 of Grapher™ from Golden Software, LLC (www.goldensoftware.com). Progressed data from all methods used in this study is available via https://doi.pangaea.de/10.1594/PANGAEA.950248.

Acknowledgments
We would like to thank the crew of RV Meteor and chief scientist Prof. Dr. Andrea Koschinsky for supporting our research at sea, Jessica Münch, Julia Fronzek and Luise Heinrich for onboard pore water sampling and Andre Mutzberg and Lisa Leist for onboard nutrient measurements. Furthermore, we would like to thank Anna-Kathrin Retschko, Regina Surberg, Anke Bleyer and Bettina Domeyer for laboratory support at GEOMAR. This work was financed by the German Research Foundation (DFG) through the Emmy Noether Research Group ICONOX (Iron Cycling in Continental Margin Sediments and the Nutrient and Oxygen Balance of the Ocean). Constructive and helpful comments of three reviewers helped us to improve the manuscript. Open Access funding enabled and organized by Projekt DEAL.

References

Adams, C. E., Wells, J. T., & Coleman, J. M. (1986). Transverse bedforms on the Amazon shelf. *Continental Shelf Research*, *6*(1), 175–187. https://doi.org/10.1016/0278-4343(86)90059-2

Alcott, L. J., Krause, A. J., Hammarlund, E. U., Bjerrum, C. J., Scholz, F., Xiong, Y., et al. (2020). Development of iron speciation reference materials for palaeoredox analysis. *Geostandards and Geoanalytical Research*, *44*(3), 581–591. https://doi.org/10.1111/ggr.12342

Aller, R. C., & Blair, N. E. (1996). Sulfur diagenesis and burial on the Amazon shelf: Major control by physical sedimentation processes. *Geo-Marine Letters*, *16*(1), 3–10. https://doi.org/10.1007/bf01218830

Aller, R. C., Heilbrun, C., Panzeca, C., Zhu, Z., & Baltzer, F. (2004). Coupling between sedimentary dynamics, early diagenetic processes, and biogeochemical cycling in the Amazon–Guianas mobile mud belt: Coastal French Guiana. *Marine Geology*, *208*(2–4), 331–360. https://doi.org/10.1016/j.margeo.2004.04.027

Aller, R. C., Mackin, J. E., & Cox, R. T. (1986). Diagenesis of Fe and S in Amazon inner shelf muds: Apparent dominance of Fe reduction and implications for the genesis of ironstones. *Continental Shelf Research*, *6*(1–2), 263–289. https://doi.org/10.1016/0278-4343(86)90064-6

Aller, R. C., Madrid, V., Chistoserdov, A., Aller, J. Y., & Heilbrun, C. (2010). Unsteady diagenetic processes and sulfur biogeochemistry in tropical deltaic muds: Implications for oceanic isotope cycles and the sedimentary record. *Geochimica et Cosmochimica Acta*, *74*(16), 4671–4692. https://doi.org/10.1016/j.gca.2010.05.008

Arndt, S., Jørgensen, B. B., LaRowe, D. E., Middelburg, J. J., Pancost, R. D., & Regnier, P. (2013). Quantifying the degradation of organic matter in marine sediments: A review and synthesis. *Earth-Science Reviews*, *123*(4), 53–86. https://doi.org/10.1016/j.earscirev.2013.02.008

Aucour, A.-M., Tao, F.-X., Moreira-Turcq, P., Seyler, P., Sheppard, S., & Benedetti, M. F. (2003). The Amazon River: Behaviour of metals (Fe, Al, Mn) and dissolved organic matter in the initial mixing at the Rio Negro/Solimões confluence. *Chemical Geology*, *197*(1–4), 271–285. https://doi.org/10.1016/S0009-2541(02)00398-4

Baldermann, A., Banerjee, S., Czuppon, G., Dietzel, M., Farkaš, J., Löhr, S., et al. (2022). Impact of green clay authigenesis on element sequestration in marine settings. *Nature Communications*, *13*(1), 1527. https://doi.org/10.1038/s41467-022-29223-6

Baldermann, A., Warr, L. N., Letofsky-Papst, I., & Mavromatis, V. (2015). Substantial iron sequestration during green-clay authigenesis in modern deep-sea sediments. *Nature Geoscience*, *8*(11), 885–889. https://doi.org/10.1038/ngeo2542

Bergquist, B. A., & Boyle, E. A. (2006). Iron isotopes in the Amazon River system: Weathering and transport signatures. *Earth and Planetary Science Letters*, *248*(1–2), 54–68. https://doi.org/10.1016/j.epsl.2006.05.004

Berner, R. A. (1970). Sedimentary pyrite formation. *American Journal of Science*, *268*(1), 1–23. https://doi.org/10.2475/ajs.268.1.1

Berner, R. A. (1984). Sedimentary pyrite formation: An update. *Geochimica et Cosmochimica Acta*, *48*(4), 605–615. https://doi.org/10.1016/0016-7037(84)90089-9

Bleil, U., Benthien, A., Böke, W., Buschhoff, H., Donner, B., Dorschel, B., et al. (1998). Report and preliminary results of METEOR cruise M 38/2: Recife—Las Palmas, 04.03.-14.04.1997. (Berichte, Fachbereich Geowissenschaften No. 95).

Blume, H. P. (1988). The fate of iron during soil formation in humid-temperate environments. In J. W. Stucki, B. A. Goodman, & U. Schwertmann (Eds.), *Iron in soils and clay minerals*. NATO ASI Series (Vol. 217). Springer. https://doi.org/10.1007/978-94-009-4007-9_21

Boyd, P. W., & Ellwood, M. J. (2010). The biogeochemical cycle of iron in the ocean. *Nature Geoscience*, *3*(10), 675–682. https://doi.org/10.1038/ngeo964

Candela, J., Beardsley, R. C., & Limeburner, R. (1992). Separation of tidal and subtidal currents in ship-mounted acoustic Doppler current profiler observations. *Journal of Geophysical Research*, *97*(C1), 769–788. https://doi.org/10.1029/91JC02569

Canfield, D. E. (1989). Reactive iron in marine sediments. *Geochimica et Cosmochimica Acta*, *53*(3), 619–632. https://doi.org/10.1016/0016-7037(89)90005-7

Canfield, D. E. (1997). The geochemistry of river particulates from the continental USA: Major elements. *Geochimica et Cosmochimica Acta*, *61*(16), 3349–3365. https://doi.org/10.1016/s0016-7037(97)00172-5

Canfield, D. E., Raiswell, R., Westrich, J. T., Reaves, C. M., & Berner, R. A. (1986). The use of chromium reduction in the analysis of reduced inorganic sulfur in sediments and shales. *Chemical Geology*, *54*(1–2), 149–155. https://doi.org/10.1016/0009-2541(86)90078-1

Canfield, D. E., & Thamdrup, B. O. (2009). Towards a consistent classification scheme for geochemical environments, or, why we wish the term 'suboxic' would go away. *Geobiology*, *7*(4), 385–392.

Cao, Y., Song, H., Algeo, T. J., Chu, D., Du, Y., Tian, L., et al. (2019). Intensified chemical weathering during the Permian-Triassic transition recorded in terrestrial and marine successions. *Palaeogeography, Palaeoclimatology, Palaeoecology*, *519*, 166–177. https://doi.org/10.1016/j.palaeo.2018.06.012

Dai, A., Qian, T., Trenberth, K. E., & Milliman, J. D. (2009). Changes in continental freshwater discharge from 1948 to 2004. *Journal of Climate*, *22*(10), 2773–2792. https://doi.org/10.1175/2008JCLI2592.1

Dale, A. W., Nickelsen, L., Scholz, F., Hensen, C., Oschlies, A., & Wallmann, K. (2015). A revised global estimate of dissolved iron fluxes from marine sediments. *Global Biogeochemical Cycles*, *29*(5), 691–707. https://doi.org/10.1002/2014gb005017

Elrod, V. A., Berelson, W. M., Coale, K. H., & Johnson, K. S. (2004). The flux of iron from continental shelf sediments: A missing source for global budgets. *Geophysical Research Letters*, *31*(12). https://doi.org/10.1029/2004gl020216

Eroglu, S., Scholz, F., Salvatteci, R., Siebert, C., Schneider, R., & Frank, M. (2021). The impact of postdepositional alteration on iron-and molybdenum-based redox proxies. *Geology*, *49*(12), 1411–1415. https://doi.org/10.1130/g49291.1

Faust, J. C., Tessin, A., Fisher, B. J., Zindorf, M., Papadaki, S., Hendry, K. R., et al. (2021). Millennial scale persistence of organic carbon bound to iron in Arctic marine sediments. *Nature Communications*, *12*(1), 275. https://doi.org/10.1038/s41467-020-20550-0

Föllmi, K. B. (1995). 160 m.y. record of marine sedimentary phosphorus burial: Coupling of climate and continental weathering under greenhouse and icehouse conditions. *Geology*, *23*(6), 503–506. https://doi.org/10.1130/0091-7613(1995)023<0503:MYROMS>2.3.CO;2

Froelich, P. _N. _, Klinkhammer, G. P., Bender, M. L., Luedtke, N. A., Heath, G. R., Cullen, D., et al. (1979). Early oxidation of organic matter in pelagic sediments of the eastern equatorial Atlantic: Suboxic diagenesis. *Geochimica et Cosmochimica Acta*, *43*(7), 1075–1090. https://doi.org/10.1016/0016-7037(79)90095-4

Gaillardet, J., Dupre, B., Allegre, C. J., & Négrel, P. (1997). Chemical and physical denudation in the Amazon River basin. *Chemical Geology*, *142*(3–4), 141–173. https://doi.org/10.1016/s0009-2541(97)00074-0

Gibbs, R. J. (1967). The geochemistry of the Amazon River system: Part I. The factors that control the salinity and the composition and concentration of the suspended solids. *GSA Bulletin*, *78*(10), 1203–1232. https://doi.org/10.1130/0016-7606(1967)78[1203:tgotar]2.0.co;2

Gibbs, R. J. (1973). The bottom sediments of the Amazon shelf and tropical Atlantic Ocean. *Marine Geology*, *14*(5), 39–45. https://doi.org/10.1016/0025-3227(73)90010-8

Harder, H. (1976). Nontronite synthesis at low temperatures. *Chemical Geology*, *18*(3), 169–180. https://doi.org/10.1016/0009-2541(76)90001-2

Hemingway, J. D., Rothman, D. H., Grant, K. E., Rosengard, S. Z., Eglinton, T. I., Derry, L. A., & Galy, V. V. (2019). Mineral protection regulates long-term global preservation of natural organic carbon. *Nature*, *570*(7760), 228–231. https://doi.org/10.1038/s41586-019-1280-6

Henkel, S., Kasten, S., Poulton, S. W., & Staubwasser, M. (2016). Determination of the stable iron isotopic composition of sequentially leached iron phases in marine sediments. *Chemical Geology*, *421*, 93–102. https://doi.org/10.1016/j.chemgeo.2015.12.003

Hepburn, L. E., Butler, I. B., Boyce, A., & Schröder, C. (2020). The use of operationally-defined sequential Fe extraction methods for mineralogical applications: A cautionary tale from Mössbauer spectroscopy. *Chemical Geology*, *543*, 119584. https://doi.org/10.1016/j.chemgeo.2020.119584

Homoky, W. B., Conway, T. M., John, S. G., König, D., Deng, F., Tagliabue, A., & Mills, R. A. (2021). Iron colloids dominate sedimentary supply to the ocean interior. *Proceedings of the National Academy of Sciences*, *118*(13), e2016078118. https://doi.org/10.1073/pnas.2016078118

Homoky, W. B., Hembury, D. J., Hepburn, L., Mills, R. A., Statham, P. J., Fones, G. R., & Palmer, M. (2011). Iron and manganese diagenesis in deep sea volcanogenic sediments and the origins of pore water colloids. *Geochimica et Cosmochimica Acta*, *75*(17), 5032–5048. https://doi.org/10.1016/j.gca.2011.06.019

Huerta-Diaz, M. A., & Morse, J. W. (1990). A quantitative method for determination of trace metal concentrations in sedimentary pyrite. *Marine Chemistry*, *29*, 119–144. https://doi.org/10.1016/0304-4203(90)90009-2

Jørgensen, B. B. (1982). Mineralization of organic matter in the sea bed—The role of sulphate reduction. *Nature*, *296*(5858), 643–645. https://doi.org/10.1038/296643a0

Karlin, R., Lyle, M., & Heath, G. R. (1987). Authigenic magnetite formation in suboxic marine sediments. *Nature*, *326*(6112), 490–493. https://doi.org/10.1038/326490a0

Kennedy, M. J., & Wagner, T. (2011). Clay mineral continental amplifier for marine carbon sequestration in a greenhouse ocean. *Proceedings of the National Academy of Sciences*, *108*(24), 9776–9781. https://doi.org/10.1073/pnas.1018670108

Koschinsky, A., Frank, M., Dittmar, T., Gledhill, M., de Rezende, C., Lodeiro, P., et al. (2018). Interactions of trace metals, DOM, and particles in the Amazon estuary and associated plume as key processes for trace metal and DOM fluxes into the Atlantic: Cruise No. M147, April 19–may 21, 2018, Las Palmas (Gran Canaria)—Belém (Brazil), 1–63. https://doi.org/10.2312/cr_m147

Kuehl, S. A., DeMaster, D. J., & Nittrouer, C. A. (1986). Nature of sediment accumulation on the Amazon continental shelf. *Continental Shelf Research*, *6*(1–2), 209–225. https://doi.org/10.1016/0278-4343(86)90061-0

Lalonde, K., Mucci, A., Ouellet, A., & Gélinas, Y. (2012). Preservation of organic matter in sediments promoted by iron. *Nature*, *483*(7388), 198–200. https://doi.org/10.1038/nature10855

Laufer-Meiser, K., Michaud, A. B., Maisch, M., Byrne, J. M., Kappler, A., Patterson, M. O., et al. (2021). Potentially bioavailable iron produced through benthic cycling in glaciated Arctic fjords of Svalbard. *Nature Communications*, *12*(1), 1349. https://doi.org/10.1038/s41467-021-21558-w

Lenstra, W. K., Hermans, M., Séguret, M. J. M., Witbaard, R., Behrends, T., Dijkstra, N., et al. (2019). The shelf-to-basin iron shuttle in the Black Sea revisited. *Chemical Geology*, *511*(3–4), 314–341. https://doi.org/10.1016/j.chemgeo.2018.10.024

Lyons, T. W., & Severmann, S. (2006). A critical look at iron paleoredox proxies: New insights from modern euxinic marine basins. *Geochimica et Cosmochimica Acta*, *70*(23), 5698–5722. https://doi.org/10.1016/j.gca.2006.08.021

Mackenzie, F. T., & Garrels, R. M. (1966). Chemical mass balance between rivers and oceans. *American Journal of Science*, *264*(7), 507–525. https://doi.org/10.2475/ajs.264.7.507

Mackin, J. E., & Aller, R. C. (1984). Processes affecting the behavior of dissolved aluminum in estuarine waters. *Marine Chemistry*, *14*(3), 213–232. https://doi.org/10.1016/0304-4203(84)90043-4

Martin, J.-M., & Meybeck, M. (1979). Elemental mass-balance of material carried by major world rivers. *Marine Chemistry*, *7*(3), 173–206. https://doi.org/10.1016/0304-4203(79)90039-2

Mayer, L. M. (1982). Retention of riverine iron in estuaries. *Geochimica et Cosmochimica Acta*, *46*(6), 1003–1009. https://doi.org/10.1016/0016-7037(82)90055-2

Meade, R. H., Dunne, T., Richey, J. E., Santos, U. D. M., & Salati, E. (1985). Storage and remobilization of suspended sediment in the lower Amazon River of Brazil. *Science*, *228*(4698), 488–490. https://doi.org/10.1126/science.228.4698.488

Michalopoulos, P., & Aller, R. C. (1995). Rapid clay mineral formation in Amazon delta sediments: Reverse weathering and oceanic elemental cycles. *Science*, *270*(5236), 614–617. https://doi.org/10.1126/science.270.5236.614

Michalopoulos, P., & Aller, R. C. (2004). Early diagenesis of biogenic silica in the Amazon delta: Alteration, authigenic clay formation, and storage. *Geochimica et Cosmochimica Acta*, *68*(5), 1061–1085. https://doi.org/10.1016/j.gca.2003.07.018

Michalopoulos, P., Aller, R. C., & Reeder, R. J. (2000). Conversion of diatoms to clays during early diagenesis in tropical, continental shelf muds. *Geology*, *28*(12), 1095–1098. https://doi.org/10.1130/0091-7613(2000)28<1095:CODTCD>2.0.CO;2

Milliman, J. D., & BARRETTO, H. T. (1975). Relict magnesian calcite oolite and subsidence of the Amazon shelf. *Sedimentology*, *22*(1), 137–145. https://doi.org/10.1111/j.1365-3091.1975.tb00288.x

Milliman, J. D., & Syvitski, J. P. M. (1992). Geomorphic/tectonic control of sediment discharge to the ocean: The importance of small mountainous rivers. *The Journal of Geology*, *100*(5), 525–544. https://doi.org/10.1086/629606

Moore, R. M., Burton, J. D., Williams, P. L., & Young, M. L. (1979). The behaviour of dissolved organic material, iron and manganese in estuarine mixing. *Geochimica et Cosmochimica Acta*, *43*(6), 919–926. https://doi.org/10.1016/0016-7037(79)90229-1

Nittrouer, C. A., Curtin, T. B., & DeMaster, D. J. (1986). Concentration and flux of suspended sediment on the Amazon continental shelf. *Continental Shelf Research*, *6*(1–2), 151–174. https://doi.org/10.1016/0278-4343(86)90058-0

Nittrouer, C. A., Kuehl, S. A., Sternberg, R. W., Figueiredo, A. G., Jr., & Faria, L. E. C. (1995). An introduction to the geological significance of sediment transport and accumulation on the Amazon continental shelf. *Marine Geology*, *125*(3–4), 177–192. https://doi.org/10.1016/0025-3227(95)00075-a

Nittrouer, C. A., Sharara, M. T., & DeMaster, D. J. (1983). Variations of sediment texture on the Amazon continental shelf. *Journal of Sedimentary Research*, *53*(1), 179–191.

Pogge von Strandmann, P. A. E., Jenkyns, H. C., & Woodfine, R. G. (2013). Lithium isotope evidence for enhanced weathering during Oceanic Anoxic Event 2. *Nature Geoscience*, *6*(8), 668–672. https://doi.org/10.1038/ngeo1875

Poulton, S. W., & Canfield, D. E. (2005). Development of a sequential extraction procedure for iron: Implications for iron partitioning in continentally derived particulates. *Chemical Geology*, *214*(3–4), 209–221. https://doi.org/10.1016/j.chemgeo.2004.09.003

Poulton, S. W., & Canfield, D. E. (2011). Ferruginous conditions: A dominant feature of the ocean through Earth's history. *Elements*, *7*(2), 107–112. https://doi.org/10.2113/gselements.7.2.107

Poulton, S. W., Fralick, P. W., & Canfield, D. E. (2010). Spatial variability in oceanic redox structure 1.8 billion years ago. *Nature Geoscience*, *3*(7), 486–490. https://doi.org/10.1038/ngeo889

Poulton, S. W., & Raiswell, R. (2000). Solid phase associations, oceanic fluxes and the anthropogenic perturbation of transition metals in world river particulates. *Marine Chemistry*, *72*(1), 17–31. https://doi.org/10.1016/s0304-4203(00)00060-8

Poulton, S. W., & Raiswell, R. (2002). The low-temperature geochemical cycle of iron: From continental fluxes to marine sediment deposition. *American Journal of Science*, *302*(9), 774–805. https://doi.org/10.2475/ajs.302.9.774

Poulton, S. W., & Raiswell, R. (2005). Chemical and physical characteristics of iron oxides in riverine and glacial meltwater sediments. *Chemical Geology*, *218*(3–4), 203–221. https://doi.org/10.1016/j.chemgeo.2005.01.007

Raiswell, R. (2006). Towards a global highly reactive iron cycle. *Journal of Geochemical Exploration*, *88*(1–3), 436–439. https://doi.org/10.1016/j.gexplo.2005.08.098

Raiswell, R., & Anderson, T. F. (2005). Reactive iron enrichment in sediments deposited beneath euxinic bottom waters: Constraints on supply by shelf recycling. In I. McDonald, A. J. Boyce, I. B. Butler, R. J. Herrington, & D. A. Polya (Eds.), *Mineral deposits and Earth evolution*. Geological Society of London. https://doi.org/10.1144/GSL.SP.2005.248.01.10

Raiswell, R., & Canfield, D. E. (1998). Sources of iron for pyrite formation in marine sediments. *American Journal of Science*, *298*(3), 219–245. https://doi.org/10.2475/ajs.298.3.219

Raiswell, R., Canfield, D. E., & Berner, R. A. (1994). A comparison of iron extraction methods for the determination of degree of pyritisation and the recognition of iron-limited pyrite formation. *Chemical Geology*, *111*(1–4), 101–110. https://doi.org/10.1016/0009-2541(94)90084-1

Raiswell, R., Hardisty, D. S., Lyons, T. W., Canfield, D. E., Owens, J. D., Planavsky, N. J., et al. (2018). The iron paleoredox proxies: A guide to the pitfalls, problems and proper practice. *American Journal of Science*, *318*(5), 491–526. https://doi.org/10.2475/05.2018.03

Roberts, A. P. (2015). Magnetic mineral diagenesis. *Earth-Science Reviews*, *151*, 1–47. https://doi.org/10.1016/j.earscirev.2015.09.010

Sayles, F. L., & Mangelsdorf, P. C., Jr. (1979). Cation-exchange characteristics of Amazon River suspended sediment and its reaction with seawater. *Geochimica et Cosmochimica Acta*, *43*(5), 767–779. https://doi.org/10.1016/0016-7037(79)90260-6

Scholz, F. (2018). Identifying oxygen minimum zone-type biogeochemical cycling in Earth history using inorganic geochemical proxies. *Earth-Science Reviews*, *184*, 29–45. https://doi.org/10.1016/j.earscirev.2018.08.002

Scholz, F., Beil, S., Flögel, S., Lehmann, M. F., Holbourn, A., Wallmann, K., & Kuhnt, W. (2019). Oxygen minimum zone-type biogeochemical cycling in the Cenomanian-Turonian Proto-North Atlantic across Oceanic anoxic event 2. *Earth and Planetary Science Letters*, *517*, 50–60. https://doi.org/10.1016/j.epsl.2019.04.008

Scholz, F., Hensen, C., Noffke, A., Rohde, A., Liebetrau, V., & Wallmann, K. (2011). Early diagenesis of redox-sensitive trace metals in the Peru upwelling area—Response to ENSO-related oxygen fluctuations in the water column. *Geochimica et Cosmochimica Acta*, *75*(22), 7257–7276. https://doi.org/10.1016/j.gca.2011.08.007

Scholz, F., Schmidt, M., Hensen, C., Eroglu, S., Geilert, S., Gutjahr, M., & Liebetrau, V. (2019). Shelf-to-basin iron shuttle in the Guaymas basin, Gulf of California. *Geochimica et Cosmochimica Acta*, *261*, 76–92. https://doi.org/10.1016/j.gca.2019.07.006

Scholz, F., Severmann, S., McManus, J., & Hensen, C. (2014). Beyond the Black Sea paradigm: The sedimentary fingerprint of an open-marine iron shuttle. *Geochimica et Cosmochimica Acta*, *127*, 368–380. https://doi.org/10.1016/j.gca.2013.11.041

Scholz, F., Severmann, S., McManus, J., Noffke, A., Lomnitz, U., & Hensen, C. (2014). On the isotope composition of reactive iron in marine sediments: Redox shuttle versus early diagenesis. *Chemical Geology*, *389*, 48–59. https://doi.org/10.1016/j.chemgeo.2014.09.009

Schwertmann, U. (1988). Occurrence and formation of iron oxides in various pedoenvironments. *Iron in soils and clay minerals*, 267–308.

Severmann, S., McManus, J., Berelson, W. M., & Hammond, D. E. (2010). The continental shelf benthic iron flux and its isotope composition. *Geochimica et Cosmochimica Acta*, *74*(14), 3984–4004. https://doi.org/10.1016/j.gca.2010.04.022

Sholkovitz, E. R. (1978). The flocculation of dissolved Fe, Mn, Al, Cu, NI, Co and Cd during estuarine mixing. *Earth and Planetary Science Letters*, *41*(1), 77–86. https://doi.org/10.1016/0012-821x(78)90043-2

Sholkovitz, E. R., & Price, N. (1980). The major-element chemistry of suspended matter in the Amazon Estuary. *Geochimica et Cosmochimica Acta*, *44*(2), 163–171. https://doi.org/10.1016/0016-7037(80)90128-3

Slotznick, S. P., Sperling, E. A., Tosca, N. J., Miller, A. J., Clayton, K. E., van Helmond, N., et al. (2020). Unraveling the mineralogical complexity of sediment iron speciation using sequential extractions. *Geochemistry, Geophysics, Geosystems*, *21*(2), e2019GC008666. https://doi.org/10.1029/2019gc008666

Spiegel, T., Vosteen, P., Wallmann, K., Paul, S. A. L., Gledhill, M., & Scholz, F. (2021). Updated estimates of sedimentary potassium sequestration and phosphorus release on the Amazon shelf. *Chemical Geology*, *560*, 120017. https://doi.org/10.1016/j.chemgeo.2020.120017

Sun, H., Xiao, Y., Gao, Y., Zhang, G., Casey, J. F., & Shen, Y. (2018). Rapid enhancement of chemical weathering recorded by extremely light seawater lithium isotopes at the Permian-Triassic boundary. *Proceedings of the National Academy of Sciences of the United States of America*, *115*(15), 3782–3787. https://doi.org/10.1073/pnas.1711862115

Tagliabue, A., Aumont, O., DeAth, R., Dunne, J. P., Dutkiewicz, S., Galbraith, E., et al. (2016). How well do global ocean biogeochemistry models simulate dissolved iron distributions? *Global Biogeochemical Cycles*, *30*(2), 149–174. https://doi.org/10.1002/2015gb005289

Tagliabue, A., Bowie, A. R., Boyd, P. W., Buck, K. N., Johnson, K. S., & Saito, M. A. (2017). The integral role of iron in ocean biogeochemistry. *Nature*, *543*(7643), 51–59. https://doi.org/10.1038/nature21058

Takayanagi, K., & Gobeil, C. (2000). Dissolved aluminum in the upper St. Lawrence estuary. *Journal of Oceanography*, *56*(5), 517–525. https://doi.org/10.1023/a:1011196826709

Taylor, S. R., & McLennan, S. (2009). *Planetary crusts: Their composition, origin and evolution* (Vol. 10). Cambridge University Press.

Ueshima, M., & Tazaki, K. (2001). Possible role of microbial Polysaccharides in nontronite formation. *Clays and Clay Minerals*, *49*(4), 292–299. https://doi.org/10.1346/CCMN.2001.0490403

Van Houten, F. B., & Purucker, M. E. (1984). Glauconitic peloids and chamositic ooids—Favorable factors, constraints, and problems. *Earth-Science Reviews*, *20*(3), 211–243. https://doi.org/10.1016/0012-8252(84)90002-3

Vorhies, J. S., & Gaines, R. R. (2009). Microbial dissolution of clay minerals as a source of iron and silica in marine sediments. *Nature Geoscience*, *2*(3), 221–225. https://doi.org/10.1038/ngeo441

Vuillemin, A., Wirth, R., Kemnitz, H., Schleicher, A. M., Friese, A., Bauer, K. W., et al. (2019). Formation of diagenetic siderite in modern ferruginous sediments. *Geology*, *47*(6), 540–544. https://doi.org/10.1130/G46100.1

Walker, J. C. G. (1984). Suboxic diagenesis in banded iron formations. *Nature*, *309*(5966), 340–342. https://doi.org/10.1038/309340a0

Wei, G.-Y., Chen, T., Poulton, S. W., Lin, Y.-B., He, T., Shi, X., et al. (2021). A chemical weathering control on the delivery of particulate iron to the continental shelf. *Geochimica et Cosmochimica Acta*, *308*(3), 204–216. https://doi.org/10.1016/j.gca.2021.05.058

Zegeye, A., Bonneville, S., Benning, L. G., Sturm, A., Fowle, D. A., Jones, C., et al. (2012). Green rust formation controls nutrient availability in a ferruginous water column. *Geology*, *40*(7), 599–602. https://doi.org/10.1130/g32959.1